International Journal of New Horizons in Physics

http://dx.doi.org/10.12785/ijnhp/010101

High-Speed Modulation of Multiple Quantum Well Laser Diodes

Moustafa F. Ahmed[1,2,*], ***Ahmed H. Bakry***[1] ***and Fwoziah T. Albelady***[1]

[1]Department of Physics, Faculty of Science, King Abdulaziz University, M.B. 20803 Jeddah 21589, Saudi Arabia.
[2]Department of Physics, Faculty of Science, Minia University, 615191 Minia, Egypt.

Received: 15 Feb 2014, Revised: 5 April 2014, Accepted: 10 April 2014
Published online: 1 July 2014

Abstract: We investigate the modulation performance of high-speed multiple-quantum-well (MQW) semiconductor lasers emitting in the wavelength of 1.55 μm. The small-signal modulation characteristics are modeled and analytical forms of the relaxation frequency and the modulation bandwidth are derived. The digital modulation characteristics under both 10 and 40 Gbps are investigated using both the return to zero (RZ) and non-return to zero (NRZ) formats of the modulation current. These modulation characteristics include the waveform of the modulated signal and frequency chirp. The results showed that under 10 Gbps, the transient chirps is almost same (62.7 GHz) under both the RZ and NRZ bit patterns, whereas it increases to 72.8 and 65.1 GHz under the NRZ and RZ bit patterns, respectively.

Keywords: semiconductor lasers; multiple-quantum-well; return to zero and non-return to zero (NRZ) formats

1 Introduction

Semiconductor lasers are key light sources in optical fiber communication systems. In these systems, the laser signal is modulated using an electrical signal by means of either direct or indirect modulation [1]. In directly-modulated communication systems, the information signal is applied directly to the laser diode in addition to the bias current. However, the transmission bit rate is limited by the resonance frequency and the modulation bandwidth frequency of the laser diode [1]. A possible approach to increase the modulation bandwidth of the laser diode is to use MQW laser diodes, which are characterized by large differential gain of the active region. An example of a 1.55 μm MQW laser is given in [2] to meet the requirement of 40 Gbps fiber transmission systems for applications in very-short-reach optical links [3]. However the intensity variation is associated with phase modulation through the linewidth enhancement factor [4]. Such phase modulation causes variation in the lasing frequency (frequency chirp) [1]. The frequency chirp increases with the increase in both the differential gain coefficient and the linewidth enhancement factor which has large values in long-wavelength semiconductor lasers [5]. Therefore, high speed 1.55 μm laser diodes are expected to have large values of the frequency chirp which manifests as broadening of the lineshape [6] and limits the fiber length in high speed fiber communication systems [7,8]. Investigations of the dynamics and chirp of the high speed laser are needful to optimize its modulation conditions for use in modern and future short reach networks that operates at transmission rates of 40 Gbps. In additions, it is important to compare the laser diode performance under NRZ and RZ modulation bit patterns.

In this paper, we model and simulate the intrinsic digital modulation characteristics of high speed 1.55 μm MQW laser diodes for use in both 10 and 40 Gbps communication systems. These characteristics include the waveform of the modulated laser signal, frequency chirp and eye diagram. We apply the present studies for both the RZ and NRZ patterns of the pseudorandom modulation bits. The Optisystem software 12.0 is used to simulate the laser characteristics under large-signal modulation. The theoretical model of analysis of these simulations is given in section 2. In sections 3 and 4, we present the results of small- and large-signal modulation of the laser using the small-signal approximation and numerical integration, respectively.

* Corresponding author e-mail: mostafa.farghal@mu.edu.eg

© 2014 NSP
Natural Sciences Publishing Cor.

2 Rate Equation Model of Laser Diode under Modulation

The rate equation model of semiconductor lasers given in section 2.2.3 is modified to account for the pseudorandom digital modulation and to include the intrinsic noise. These rate equations take the form [9]

$$\frac{dN}{dt} = \frac{I(t)}{qV} - \frac{N}{\tau_e} - a_0 v_g \frac{N - N_g}{1 + \varepsilon S} + F_N(t) \quad (1)$$

$$\frac{dS}{dt} = \Gamma a_0 v_g \frac{N - N_g}{1 + \varepsilon S} - \frac{S}{\tau_p} + \frac{\Gamma \beta_{sp} N}{\tau_p} + F_S(t) \quad (2)$$

$$\frac{d\theta}{dt} = 2\pi \Delta f = \frac{\alpha}{2} \Gamma a_0 v_g (N - N_{th}) + F_\theta(t) \quad (3)$$

The current term $I(t)$ of equation (1) varies with time as;

$$I(t) = I_b + I_m \Psi_m(t) \quad (4)$$

where I_b is the bias current, is the modulation current, and $\Psi_m(t)$ represents the shape of the current signal, either the RZ or NRZ pattern.

The last terms $F_N(t)$, $F_S(t)$ and $F_\theta(t)$ in equations (1) and (2) are Langevin noise terms and are added to the equations to take into account the quantum noises on the photon and electron densities and optical phase, respectively [10]. These noises are caused by random fluctuations in the electron and photon recombination and generation processes, which result in instantaneous time variations in the electron and photon densities [10]. The time variation for the optical power is determined from the photon number $S(t)$ via the relationship [1]:

$$P_T = \frac{V \eta_0 h f S}{2 \Gamma \tau_p} \quad (5)$$

where η_0 is the differential quantum efficiency, f is the optical frequency, and h is the Planck's constant.

3 Numerical Calculations

Rate equations (1) and (3) are solved numerically by means of the fourth-order Runge-Kutta method [11]. Pseudorandom square pulses with both the RZ and NRZ patterns are assumed to be $\Psi_m(t)$ in equation (4). These square pulses are generated by a pseudorandom bit sequence (PRBS) generator. The used bit-sequence length is $2^9 - 1$, and the bit duration or the bit slot is $T_b = 1/B$, where B is the bit rate. In the present work, the bit rate is set to be $B = 10$ and 40 Gbps, which correspond to $T_b = 100$ and 25 ps, respectively. In the integration process, each bit is divided into 64 samples, which results in a time step of ΔT 1.6 and 0.4 ps for the cases of 10 and 40 Gbps modulations, respectively. The calculations are applied to an *InGaAsP* MQW-distributed feedback (DFB) laser emitting with λ =1.55 μm using the parametric values given in Table ((1)) [3]. The non-radiative recombination processes in this long-wavelength laser are taken into account in the calculation of the spontaneous emission life time τ_e via the relationship [12]

$$\frac{1}{\tau_e} = A_{nr} + B_r N + C_{AUG} N^2 \quad (6)$$

where A_{nr} and C_{AUG} are rates of nonradiative recombination due to crystal imperfections and the Auger processes, respectively, and B_r is the rate of radiative recombination. The bias and modulation currents are set to be I_b = 92 mA and I_m = 90 mA, respectively, which correspond to the modulation bandwidth of $f3dB =$ observed in experiments on MQW DFB laser diodes [3, 13]. These currents are well above the threshold level in order to avoid contribution of the noisy spontaneous emission process to the lasing action. These currents correspond to a transmitter power of P_T = 11 Bm. The proposed PIN photodetector is used with a low-pass Bessel filter of order 4 [14]. Typical values of the parameters of this device are given in Table (1). The techniques of instantaneous generation of the Langevin noise sources $F_N(t)$, $F_S(t)$ and $F_\theta(t)$ can be found in [10].

4 Results and Discussion

4.1 Light-current (L-I) characteristics

The most important characteristic of the laser diode to be measured is the amount of light it emits when current is injected into the active region. This generates the output light versus input current curve, more commonly referred to as the (L-I) characteristics. Theoretically this curve can be generated by calculating the steady state values of the emitted power at a relatively long time as a function of the injection current. Figure (1) plots the calculated L-I curve, showing that the L-I characteristics can be divided broadly into two parts; namely, the spontaneous and the stimulated regions. In the region of low current, any radiation generated is due to the spontaneous emission where the laser behaves like a light emitting diode. In this region, the current density in the active region is not enough to support lasing. As the injected current is increased, the threshold current I_{th} is reached and the laser begins to emit stimulated radiation, which is the onset of laser action, and the light output then increases very rapidly with increasing the current [12, 15].

From the L-I curve, the threshold current I_{th} can be obtained, which is a very important parameter since it is strictly related to the power consumption of the laser. I_{th} is obtained by extracting the linear relation of the stimulated emission and determining its interception with the current axis. The calculated value of the threshold current is I_{th} = 10 mA. Also from the L-I curves, we determine the slope efficiency which describes how well

© 2014 NSP
Natural Sciences Publishing Cor.

Table 1: Typical values of the DFB MQW laser diode and PIN photodiode parameters [3]

Symbol	Definition	Value
Laser parameters		
λ	Wavelength	$1.55\mu m$
V	Active layer volume	$3x10^{-11}cm^3$
υ_g	Group velocity	$8.33x10^9 cm/s$
η_0	Quantum efficiency	0.255
a_0	Differential gain coefficient	$9.9x10^{-16}cm^2$
N_g	Carrier density at transparency	$1.23x10^{18}cm^{-3}$
α	Linewidth enhancement factor	3.5
Γ	Mode confinement factor	0.2
A_{nr}	recombination coefficient	$10^8 s^{-1}$
B_r	recombination coefficient	$3.5x10^{-10}cm^3/s$
C_{AUG}	recombination coefficient	$7.5x10^{-29}cm^6/s$
τ_p	Photon lifetime	$1.69x10^{-12}s$
β_{sp}	Spontaneous emission factor	$3x10^{-5}$
ε	Gain compression coefficient	$2.77x10^{-17}cm^3$
PIN Photodetector		
R	Responsivity	$1A/W$
I_{th}	Thermal noise	$10^{-22}W/Hz$
I_d	Dark current	$10nA$

the light output power of the laser responds to the increase in the injection current [16]. The calculated slope efficiency is h =8.18x10^{-4} W/A.

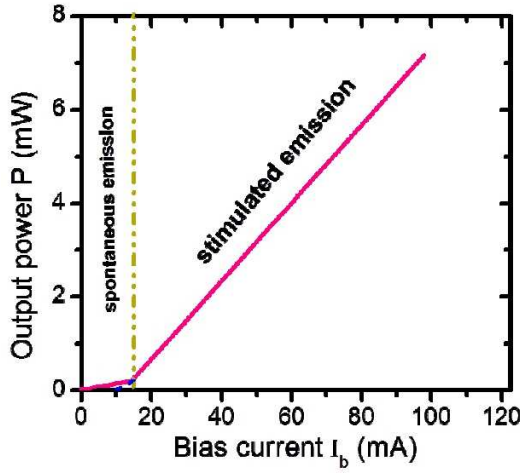

Fig. 1: The (L-I) characteristics of the MQW DFB laser. I_{th} = 10 mA and $\eta_0 = 8.18\times10^{-4}W/A$.

4.2 Small-signal modulation analysis

In this section, we present small-signal analysis of the sinusoidal modulation of the present semiconductor laser. This analysis is useful for obtaining analytic solutions of the laser rate equations under small-signal modulation and relating the modulation characteristics to the laser parameters and the modulation conditions. Under the small-signal modulation analysis, the laser is biased above threshold $I_b > I_{th}$ and modulated such that $I_m < I_b - I_{th}$ [2]. For such analysis, the noise sources are dropped from rate equations (1- 3). The injection current $I(t)$ in equation (1) is defined in the sinusoidal form:

$$I(t) = I_b + I_m \cos(\Omega_m t) \tag{7}$$

with $I_m << I_b - I_{th}$ This equation can be re-written as:

$$I = I_b + \left[\frac{I_m}{2}\exp(J\Omega_m t + C.C\right] \tag{8}$$

where c. c. indicates the complex conjugate, and the angular frequency Ω_m. is related to the modulation frequency f_m as $\Omega_m = 2\pi f_m$. In the small-signal analysis, both $S(t)$ and $N(t)$ are separated also into a bias and modulation terms as:

$$N(t) = N_b + \left[\frac{N_m}{2}\exp(J\Omega_m t + C.C\right] \tag{9}$$

$$S(t) = S_b + \left[\frac{S_m}{2}\exp(J\Omega_m t + C.C\right] \tag{10}$$

such that $N_m << N_b$ and $S_m << S_b$. By substituting equations (8-10) into the rate equations, comparing both sides of the obtained equations, one can obtain a pair of equations for the bias components and another pair of equations for the modulation components. By neglecting the higher harmonics, the equations of the bias components are:

$$\upsilon_g a_0 \frac{N_b - N_0 S_b}{1+\varepsilon S_b} + \frac{I_b}{qV} - \frac{N_b}{\tau_e} = 0 \tag{11}$$

© 2014 NSP
Natural Sciences Publishing Cor.

$$\Gamma \upsilon_g a_0 \frac{N_b - N_0 S_b}{1+\varepsilon S_b} - \frac{S_b}{\tau_p} + \frac{\Gamma R_{sp}}{V} = 0 \tag{12}$$

and the equations of the modulation components are:

$$-[\Gamma_S + j\Omega_m]S_m + \Gamma \upsilon_g a_0 N_m \frac{S_b}{1+\varepsilon S_b} = 0 \tag{13}$$

$$-[\Gamma_N + j\Omega_m]N_m - \upsilon_g a_0 S_m \frac{N_b - N_0}{1+\varepsilon S_b} + \frac{I_m}{qV} = 0 \tag{14}$$

where

$$\Gamma_N = 2\pi\gamma_N = -\Gamma \upsilon_g a_0 \frac{(N_b - N_0)}{1+\varepsilon S_b} + \frac{1}{\tau_e} \tag{15}$$

$$\Gamma_S = 2\pi\gamma_S = \upsilon_g a_0 \frac{S_b}{1+\varepsilon S_b} + \frac{1}{\tau_P} \tag{16}$$

are the damping rates of $N(t)$ and $S(t)$ respectively. The modulation component N_m of $N(t)$ is determined from equation (8) as a function of S_m as,

$$N_m = \frac{\frac{I_m}{qV} - \upsilon_g a_0 \frac{(N_b - N_0)S_m}{1+\varepsilon S_b}}{j\Omega_m + \Gamma_N} \tag{17}$$

The component S_m is then determined by substituting for N_m into equation (13),

$$S_m(\Omega_m) = \frac{\Gamma \upsilon_g N_b - a_0 \frac{S_b}{1+\varepsilon S_b}\frac{I_m}{qV}}{\Omega_r^2 + 2j\Omega_m\Gamma_r - \Omega_m^2} \tag{18}$$

where $\Omega_r = 2\pi f_r$ and Γ_r are the relaxation circular frequency and the damping rate, respectively, and are given by:

$$\Omega_r^2 = (2\pi f_r)^2 = \Gamma_N\Gamma_S + \Gamma \upsilon_g^2 a_0^2 \frac{(N_b - N_0)S_b}{(1+\varepsilon S_b)^2} \tag{19}$$

$$\begin{aligned}\Gamma_r &= \frac{1}{2}(\Gamma_N + \Gamma_S) \\ &= \frac{1}{2}(\upsilon_g a_0 \frac{S_b}{1+\varepsilon S_b} + \frac{1}{\tau_p} - \Gamma \upsilon_g a_0 \frac{N_b - N_0}{1+\varepsilon S_b} + \frac{1}{\tau_e})\end{aligned} \tag{20}$$

4.2.1 Modulation response

The transfer function from current modulation to a variation in the optical power defines the small-signal modulation response [2]. This response $H_m(\Omega_m)$ at a given modulation frequency Ω_m is defined as the ratio of the modulated photon number $S_m(\Omega_m)$ to the non-modulated photon number $S_m(0)$. $H_m(\Omega_m)$ is then given by

$$\begin{aligned}H(\Omega_m) &= \frac{S_m(\Omega_m)}{S_m(0)} \\ &= \frac{\Omega_r^2}{\Omega_r^2 + 2j\Omega_m\Gamma_r - \Omega_m^2} \\ &= \frac{1}{1 + 2j\Omega_m\frac{\Gamma_r}{\Omega_r^2} - \frac{\Omega_m^2}{\Omega_r^2}}\end{aligned} \tag{21}$$

4.2.2 Modulation bandwidth

It is defined as the frequency at which the response $|H_m(\Omega_m)|$ is equal to one half of its flat part. The modulation bandwidth, or the 3dB frequency $f_{3dB} = \Omega_{-3dB}/2\pi$, decides the upper modulation frequency of the semiconductor laser. f_{3dB} is then calculated from:

$$f_{3dB} = \frac{1}{2\pi}\sqrt{(\Omega_r^2 - 2\Gamma_r^2) + 2\sqrt{(\Omega_r^2 - \Gamma_r^2)^2 + \Omega_r^2\Gamma_r^2}} \tag{22}$$

Figure (2) plots the frequency spectra of the modulation response $|H_m(f_m)|$ when the bias current is set to be I_b =2, 5 and 10 I_{th}. The figure shows that $|H_m(f_m)|$ is pronounced at the modulation frequency $f_{m(peak)} \approx f_r$. The increase in I_b is associated with a shift of the response peak to higher modulation frequencies, a decrease in the response peak, and broadening of the spectrum around the peak frequency.

The response of $|H_m(f_m)|$ could be interpreted by dividing it into three regimes: the plateau, peak, and declining region [16]. When $f_m << f_r$, the charge carriers follow the time variation of the injection current and the laser keeps the CW operation, which results in a flat response. In the vicinity of the response peak, the carriers interact with the photons in similar manner to the laser transients. The laser resonance is then a result of complete phase synchronization between the carriers and photons. The declining portion of $|H_m(f_m)|$ is due to the retard of the phase of the photon field lags behind the phase of the injection current.

The key point in increasing the modulation speed by increasing the differential gain coefficient a_0 is illustrated in figure(3).

The figure shows the increase in f_{3dB} with the increase in a_0. In this figure the bias current is I_b = 92 *mA*. The figure indicates that f_{3dB} = 12.4 GHz for conventional DFB lasers with a_0 = 2.5$\times$ 10^{-16} cm^2, and increases to f_{3dB} = 24.2 GHz for the present laser with a_0 =9.9 $\times$ 10^{-20} cm^2.

Figure(4) plots variation of f_{3dB} with the bias current I_b when $a_0 = 9.9 \times 10^{-20} cm^2$. The figure shows that f_{3dB} increases monotonically with the increase in I_b; f_{3dB} increases from 8 to 22.8 *GHz* when I_b increases from 20 to 80 *mA*. When I_b = 100 *mA*, f_{3dB} is 26 *GHz*, which is close to the reported value ($\sim$ 27*GHz*) for lasers with almost similar parameters [3,13]. This slight difference in f_{3dB} may be because the electrical parasitic is not included in the present model of analysis.

4.3 Large-signal analysis

In this subsection, we present the simulation results of digital modulation of the semiconductor laser. The results correspond to modulation at both bit rates of $B = 10$ and 40 *Gbps*.

© 2014 NSP
Natural Sciences Publishing Cor.

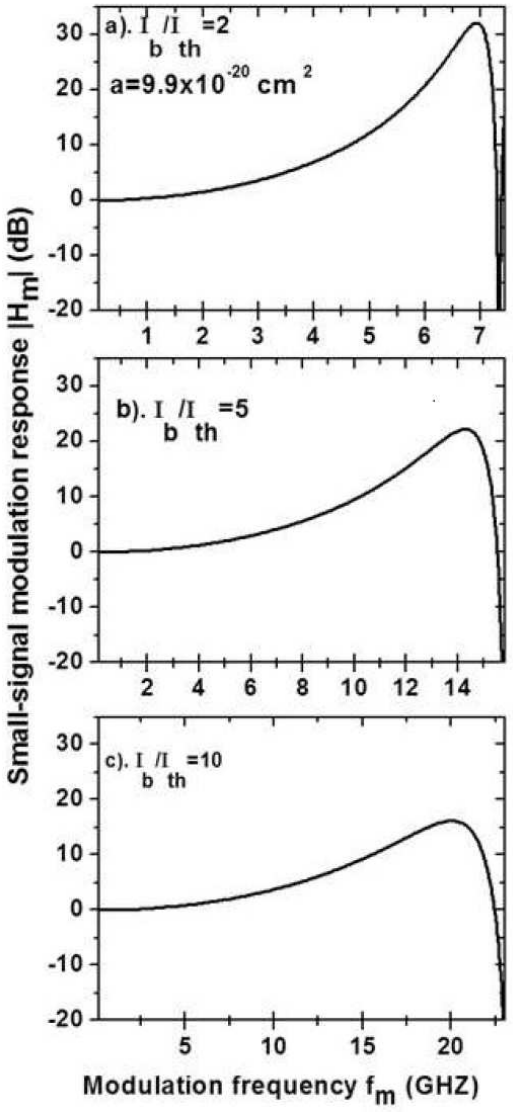

Fig. 2: Spectra of $|H_m(f_m)|$ when $I_b = 2,5$and $10I_{th}$. The peak value of $|H_m(f_m)|$ decreases with increasing I_b.

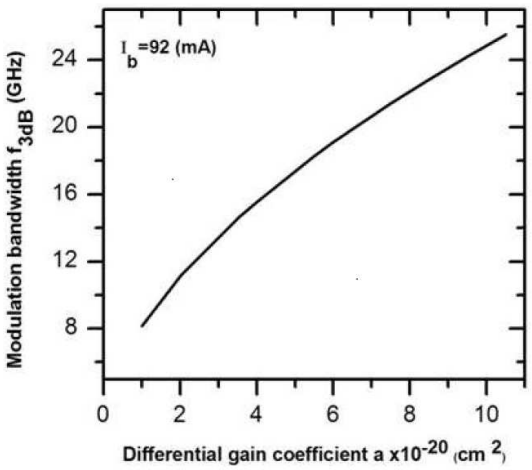

Fig. 3: Variation of f_{3dB} with with differential gain coefficient a_0 when $I_b = 92mA$.

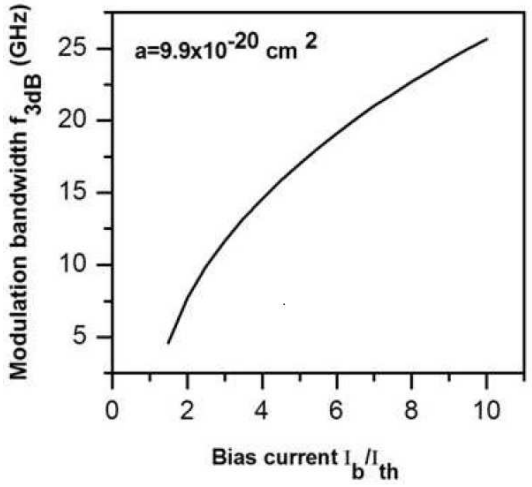

Fig. 4: Variation of the modulation bandwidth f_{3dB} with I_b when a_0= 9.9$\times$ 10^{-20} cm^2. f_{3dB}increases with the increase ofI_b

In these calculations the noise sources in equations (1) and (3) are taken into account. Examples of the simulated signal power $P(t)$ and chirp Δf of the laser when $B = 10Gbps$ under the NRZ and RZ modulation patterns are given in figures (5(a) and (5(b)), respectively. The figures show the ON/OFF modulation of the laser power and chirp. Both the power and chirp responses are characterized by the relaxation oscillations in both the ”1” and ”0” bits when preceded by opposite bits.

The shown fluctuations are manifestation of the quantum intensity and phase noises of the laser [17]. These effects are more pronounced in figure (5(b)) of the RZ pattern as the “1” bits return to the “0” level at the mid-point of the bit slot.

The figures show that the rising and falling edges of the pulse have different frequencies. The difference between these two frequencies defines the ”transient chirp” [18]. This transient chirp is induced by the relaxation oscillations, which result in transient variations in the refractive index of the active region. In the steady state, the frequency difference between the “1” and “0” levels defines the “adiabatic chirp” [18]. The figures indicate that the chirp associated with the intensity modulation is both transient and adiabatic. It is shown also that the laser chirp is blue under both modulation patterns. The transient chirps are almost same (62.68 and 62.77 GHz) under both the NRZ and RZ patterns.

Figures (6a and 6b) plot the corresponding signal power and chirp of the laser when the bit rate B is

© 2014 NSP
Natural Sciences Publishing Cor.

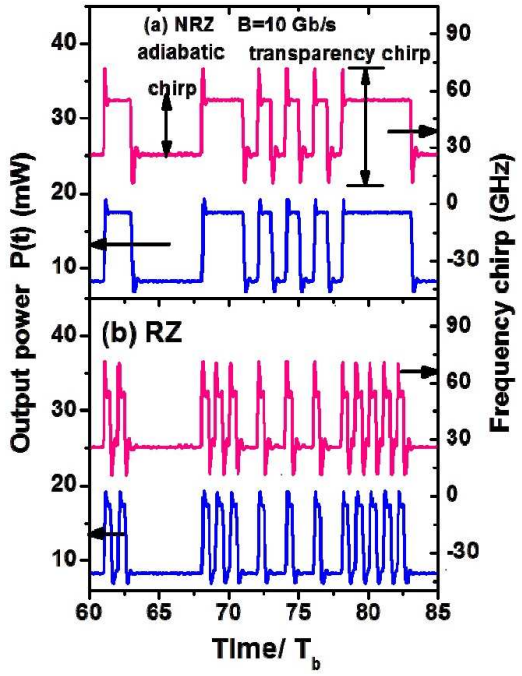

Fig. 5: Modulated waveform and chirp of the laser signal when $B = 10Gbps$ for (a) NRZ and (b) RZ modulation patterns.

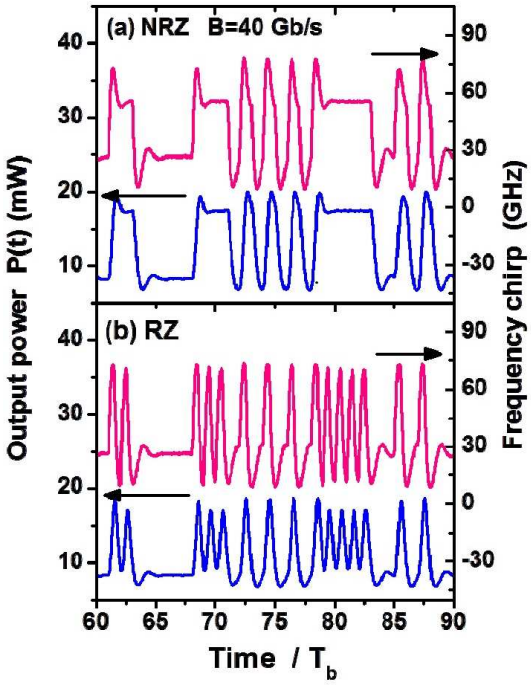

Fig. 6: Modulated waveform and chirp of the laser signal when B = 40 Gbps for (a) NRZ and (b) RZ modulation patterns.

increased to 40 Gbps under the NRZ and RZ modulation patterns, respectively. Figure (6a) shows that the signal is more broadened within the single modulation bits; the rise and fall times of the bits become longer. In additions, figure (6b) shows fluctuations in the average power of both the "0" and "1" bits, which is a pseudorandom bit-pattern effect and is induced due to the different history of the "0" bits preceding every "1" bit [17,19]. These effects are more enhanced in the waveforms of the RZ modulated power. Also, it is seen that the adiabatic chirp is hardly defined and the transient chirp becomes dominant under the RZ modulation. The transient chirp increases to 72.8 and 65.1 GHz under the NRZ and RZ modulation patterns, respectively.

The calculated frequency chirp under the NRZ pattern is slightly larger than the value of 48 GHz measured by Sato et al. [3]. This difference may be because the electrical parasitic are not taken into account in the present calculations.

5 Conclusions

We modeled and simulated the modulation characteristics of high speed quantum-well 1.55 μm laser diodes under the high bit rates of 10 and 40 Gbps. The study included both the RZ and NRZ modulation bit patterns. We investigated the intrinsic modulation characteristics of the laser, including the modulated waveform and the transient chirps. The results showed that the modulation bandwidth f_{3dB} increases with the increase in the differential gain coefficient; f_{3dB} is 12.4 GHz for conventional lasers diodes with $a_0 = 2.5 \times 10{-}16$ cm^2, and increases to f_{3dB} = 24.2 GHz for the present high-speed laser with $a_0 = 9.9 \times 10^{-20}$ cm^2. f_{3dB} increases also with the increase in the bias current. Under digital modulation, the laser power and chirp exhibit the ON/OFF modulation associated with relaxation oscillations in both the "1" or "0" bits when preceded by opposite bits.

The waveform has fluctuations due to the intensity and phase noises of the laser. Under modulation with 10 Gbps, these effects are more pronounced in the RZ bit pattern. The frequency chirp associated with the intensity modulation is both transient and adiabatic. The laser chirp is blue under both the NRZ and RZ bit patterns. The transient chirps are almost same ($\sim$62.7 GHz) under both the RZ and NRZ bit patterns. Under 40 Gbps modulation, the laser signal is more broadened within the single modulation bits. The fluctuations in the average power of both the "1" and "0" bits are due to both the intensity noise and the pseudorandom bit-pattern effect. The latter is more enhanced in the waveforms of the RZ modulated power. The adiabatic chirp is hardly defined and the transient chirp becomes dominant under the RZ bit pattern. The transient chirp is 65.1 and 72.8 GHz under the RZ and NRZ modulations bit patterns, respectively.

© 2014 NSP
Natural Sciences Publishing Cor.

References

[1] G. P Agrawal, *Optical Fiber Communication Systems* (New York : Van Nostrand Reinhold), (2003).
[2] K. Petermann, *Laser diode modulation and noise*, Dordrecht: Kluwer Academic Publishers, (1988).
[3] K. Sato, S. Kuwahar, and Y. Miyamoto, *Journal of Lightwave Technology*, **23**, 3790-3797, (2005).
[4] ITU-T draft recommendation G.693,2001.
[5] C. H Henry, *IEEE Journal of Lightwave Technology*, **4**, 298–311, (1986).
[6] M. Osinski, and J. Buus, *IEEE Journal of Quantum Electrons* , **23**, 9-29, (1987).
[7] P. Krehlik, *Optoelectrons Review*, **15**, 71-77, (2007).
[8] M. Ahmed, *International Journal of Numerical Modelling and Simulation*, **17**, 147-163, (2004).
[9] J. C Cartledge, and G. S. Burly, *IEEE Journal of Lightwave Technology*, **7**, 568-573, (1989).
[10] M. Ahmed, M. Yamada, and M. Saito, IEEE Journal of Quantum Electrons , **37**, 1600-1610, (2001).
[11] R. L. Burden, J. D. Faires, and A. C. Reynolds, *Numerical analysis*, Boston: PWSKent Pub. Co., (1981).
[12] G. P. Agrawal, and N. K. Dutta, *Semiconductor lasers*, New York: Van Nostrand Reinhold, 1993.
[13] K. Sato, S. Kuwahara, Y. Miyamoto, and N. Shimizu, *IEEE Journal of Quantum letters*, **38**, 816-817, (2002).
[14] N. Suzuki, and T. Ozeki, *IEEE Journal of Lightwave Technology*, **11**, 1486-1494, (1994).
[15] G. DanG, *Design, Fabrication, and characterization of 850 nm vertical cavity surface emitting lasers*, Ph. D. Thesis, University of Florida, USA, (2001).
[16] C. Y. Wu, *Analysis of high-speed modulation of semiconductor lasers by electron heating*, M. Sc. Thesis, University of Toronto, Canada, (1995).
[17] M. Ahmed, M. Yamada, and S. W. Z Mahmoud, *Journal of Applied Physics*, **101**, 3119-3126, (2007).
[18] M. Ahmed, S. W. Z Mahmoud, and A. Mahmoud, *Pramana Journal of Physics*, **79**, 1443-1456, (2012).
[19] M. Ahmed, *Indian Journal of Physics*, **86**, 1013-1020, (2012).

© 2014 NSP
Natural Sciences Publishing Cor.